Journal of Applied Polymer Science

Melt Spinning and Drawing of Polyethylene Nanocomposite Fibers with Organically Modified Hydrotalcite

Luca Fambri,[1,2] Izabela Dabrowska,[1] Alessandro Pegoretti,[1,2] Riccardo Ceccato[1,2]

[1]Department of Industrial Engineering, University of Trento, via Mesiano 77, 38123, Trento, Italy

[2]National Interuniversity Consortium of Materials Science and Technology (INSTM), Via G. Giusti 9, 50121, Firenze, Italy

Correspondence to: L. Fambri (luca.fambri@unitn.it).

ABSTRACT: Fibers of high density polyethylene (HDPE)/organically modified hydrotalcite (LDH) were produced by melt intercalation in a two-step process consisting of twin-screw extrusion and hot drawing. The optimum drawing temperature was 125°C at which the draw ratios up to 20 could be achieved. XRD analysis revealed intercalation with a high degree of exfoliation for the composites with 1–2% of LDH. Higher thermal stability of nanofilled fibers was confirmed by TGA analysis. DSC data indicated that dispersed LDH particles act as a nucleating agent. Crystallization kinetics of the HDPE matrix in the composite fibers is characterized by two transition temperatures, that is, for Regimes I/II at 123°C and for Regimes II/III ranging between 114–119°C as a function of the nanocomposite composition. Fibers with 1–2% of LDH show for the drawing ratios up to 15 a higher elastic modulus, 9.0–9.3 GPa (with respect to 8.0 GPa of the neat HDPE), maintain tensile strength of 0.8 GPa and deformation at break of 20–25%. © 2013 Wiley Periodicals, Inc. J. Appl. Polym. Sci. **2014**, *131*, 40277.

KEYWORDS: fibers; polyolefins; nanoparticles; nanowires and nanocrystals; mechanical properties; properties and characterization

Received 30 August 2013; accepted 9 December 2013

DOI: 10.1002/app.40277

INTRODUCTION

Polymer fibers are widely used for various textile applications, such as automotive, carpets, geotextile, sail, or as reinforcements in composite materials. The most common polymers used for melt spinning are polypropylene, polyethylene, polyamides, or polyethylene terephthalate. The interest in the production of oriented polymers with high stiffness and strength dates back to 1960–1970. In the case of polyethylene drawn films Treloar estimated the Young's modulus of about 200 GPa and tensile strength of about 3 GPa.[1] However, molecular alignment achieved after melt spinning and drawing was much lower than predicted, as described by White et al. and in references therein.[2] The development of high modulus polyethylene fibers was presented in the pioneer research of Andrews and Ward, where a direct correlation between the draw ratio and modulus was established.[3] For instance, after increasing draw ratio from 7 to 13, Young modulus of cold-drawn fibers rose from 4 GPa to 20 GPa. Capaccio and Ward comparing the drawing behavior of several commercial polyethylenes observed the best results for polymers with low molecular weight and narrow distribution, analogously to the conclusions of White and coworkers.[2,4] Nowadays polyolefins for fiber spinning have reached an extensive application, not only for economic reason but also for easy processability, excellent melt dyeability, and low moistures absorption.[5–7]

Along with melt spinning, polyolefin fibers were produced by other processing and drawing methods, for example, solid-state hot drawing, solid-state extrusion, gel-spinning of UHMWPE.[8–10] Solid-state deformation was used by Ward and coworkers, who succeeded in stretching polymers in the solid state at temperatures sufficient to permit molecular mobility of polyethylene; thus, they obtained Young's moduli of 70 GPa and tensile strength of 1.5 GPa at very high draw ratios (greater than 30).[11] Melt spinning remains widely used processing method despite of the fact that that mechanical properties of produced fibers are lower than those of the gel-spun fibers.[5]

The challenge to produce stronger, tougher, light-weight materials continues apace, being driven by demands for property improvements, economy, and material availability. In order to improve polymer properties, the introduction of small amount of inorganic nanofillers in polymer matrices is an interesting method, as it is evident that nanocomposites offer similar or better properties at significantly lower filler loading levels than materials with conventional fillers. The addition of nanofillers to polymers makes possible to produce composite materials with improved mechanical and barrier properties, flame retardancy, electrical conductivity, and so on.[12]

Recent literature evidences a lot of progress in the nanofilled bulk materials; on the contrary, there are relatively a few

Table I. Designation and Composition of the HDPE Nanocomposite Fibers

Material	Hydrotalcite [%]	HDPE [%]	Compatibilizer HDPE-*g*-MA [%]	Screw speed [rpm]	Output [g/h]
HDPE	0	100	0	5	140
LDH-0.5	0.5	99	0.5	4.5	141
LDH-1	1	98	1	5	142
LDH-2	2	96	2	4	137
LDH-3	3	94	3	3	138

publications on fibers made of nanofilled polyolefins. For instance, PP fibers were produced with various types of nanofillers, for example, layered silicates, carbon nanotubes, and montmorillonite.[13–18] In the case of HDPE, composites fibers containing calcium carbonate, carbon nanotubes, silica, and layered silicates were reported.[19–25] Owing to the alignment of the nanofiller particles along the strain direction, which induced a stronger interfacial load transfer, enhanced stiffness, and tensile strength of the composite fibers were achieved.[20–24]

Recently many articles on synthetic layered double hydrotalcite (LDH) have been published. [26–34] LDH is a synthetic clay produced in a broad range of chemical compositions. Moreover, since the chemical composition can be precisely controlled, these materials can find applications where the chemical purity is required, for example in food, medical, and microelectronic industries.[33] In general, LDH has a layered structure similar to silica clays, but the layers positively charged with an anionic interlayer gallery can be exchanged by bulk organic anions; when the interlayer distance is increased, polymer chains can intercalate into the gallery and thus nanocomposites with an intercalated and/or exfoliated morphology can be obtained.[26,27,29,34]

Commercially available grades are based on magnesium aluminum hydroxides. In this article we have used organically modified hydrotalcite characterized by the enlarged interlayer distance of the pristine clay, increased hydrophobic nature and decreased interaction between platelets to facilitate dispersion.[29] If properly processed, the organically modified hydrotalcite can easily be melt dispersed into a polymer and exfoliated forming a true nanocomposite resulting in improved properties such as thermo-mechanical, flame retardant, barrier and rheological (better thermoforming properties).[28–32]

In our previous paper we have described the compounding of hydrotalcite with HDPE (either internal mixing or mixing in twin-screw extruder) and the preliminary melt spinning of fibers and drawing at 100°C.[35] In this article, the production of polyethylene/organically modified hydrotalcite fibers was developed and detailed on a wider scale. In particular, the effects of the drawing temperature (between 100 and 140°C) and of the draw ratio (up to 20) are reported. The effects of the fiber composition and of the drawing ratio on resulting morphology (SEM) and level of intercalation/exfoliation (XRD) have been studied. Mechanical and thermal measurements of the fibers have been used to evaluate the beneficial effects of hydrotalcite with regard to its concentration and processing procedure.

EXPERIMENTAL

Materials

Fine powder of high density polyethylene HDPE Eltex® A4009 (melt flow rate 0.85 dg/min at 190°C/2.16 kg; density 0.96 g/cm^3) was supplied by BP Solvay (Brussels, Belgium).

Masterbatch pellets at 12% by weight of synthetic hydrotalcite organically modified with fatty acid, Perkalite F100 (Akzo-Nobel, CAS number 39366-43-3 and 67701-03-5; density 1.35–1.40 g/cm^3) and containing 12% by weight of maleated polyethylene HDPE-*g*-MA as compatibilizer, was provided from Clariant Masterbatches S.p.A.-Italy. Masterbatch was dried for 24 h in vacuum oven at 90°C before processing. Nanocomposites were designated as hydrotalcite abbreviation (LDH) and the filler content. As an example, LDH-1 indicates a nanocomposite sample filled with 1 wt % of hydrotalcite.

Fiber Spinning

Monofilament fibers were produced by means of Thermo Haake PTW16 intermeshing corotating twin screw extruder (screw diameter 16 mm, L/D ratio 25, rod die diameter 1.65 mm) that performed both compounding and spinning (the composition is given in Table I). The temperature profile along the screw was gradually increased (T1 = 130°C, T2 = 200°C, T3 = 210°C, T4 = 220°C) up to the rod die (T5 = 220°C). The spun fibers were fast cooled in water at room temperature in order to eliminate orientation and drawing of the fibers immediately after the extrusion, and wrapped around a rotating cylinder (40 mm diameter) rotating at 67 rpm. To obtain fibers with diameter of 500 μm, the screws rotation speed was fixed in the range 3–5 rpm depending on the material composition.

Fiber Drawing

As spun fibres were drawn in a hot-plate drawing apparatus 1.4 m length (SSM-Giudici srl, Galbiate, LC, Italy). Three different temperatures 100°C, 125°C, and 140°C, a constant feeding rate of 1.2 m/min and various collecting rates were selected. Drawn fibers were distinguished in dependence on the draw ratio (DR) that is defined as the ratio between the cross section of the initial (S_i) and final fiber (S_f) according to eq. (1)

$$DR = \frac{S_i}{S_f} = \left(\frac{D_i}{D_f}\right)^2 \quad (1)$$

where D_i and D_f are the initial and final diameter of the fiber. The diameter of the fiber was measured by using an optical microscope connected to image processing software (ImageJ®).

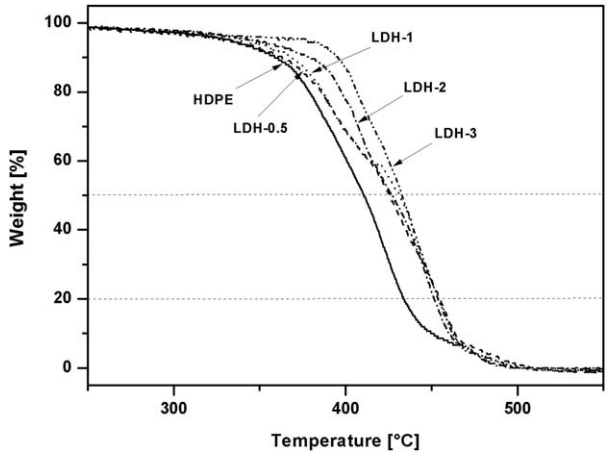

Figure 1. TGA thermograms of the neat HDPE and HDPE-LDH nanocomposite fibers with various nanofiller concentrations.

Fiber Characterization

Thermogravimetric analysis (TGA) was performed by using thermobalance Mettler TG 50 on as-spun fibers of about 15 mg in air flow (100 mL/min) at a heating rate of 10°C/min in the range 50–600°C. The temperatures at 2% and 5% of mass loss, the onset temperature (intersection between the tangent at 200°C and the tangent at the inflection point), and the temperature of the inflection point were evaluated.

Differential scanning calorimetry (DSC) analyses were performed by using a Mettler DSC30 calorimeter. The experiments were performed on fiber samples of about 15 mg in crucible of 160 μL. Crystallization kinetics of HDPE nanocomposites was studied in the nonisothermal mode from 200°C during cooling at different cooling rates from −0.3 up to −40°C/min and registering the crystallization temperature (T_c). Melting temperature, crystallization temperature, and crystallinity of as-spun and drawn fibers were studied in a heating–cooling–heating cycle at ±10°C/min in the range 0–200°C under flushing nitrogen at 100 mL/min. The crystallinity of polyethylene X_{HDPE} was calculated according to eq. (2) by normalizing the melting enthalpy ΔH_i with respect to 293 J g^{-1} (the standard enthalpy of the full crystalline polyethylene) and the weight fraction of nanofiller f.[36]

$$X_{HDPE} = 100 \frac{\Delta H_i}{293 \times (1-f)} \quad (2)$$

Scanning electron microscopy (SEM) images were obtained by using a Philips® XL30 environmental scanning electron microscopy, at an acceleration voltage between 15 and 30 kV. Samples were fractured in liquid nitrogen.

X-rays diffraction (XRD) was collected by using a Rigaku III D-Max diffractometer, in a θ-2θ Bragg-Brentano geometry with a graphite monochromator in the diffracted beam (monochromatic radiation CuK_α line with $\lambda = 1.54056$ Å), with the following parameters can range: 1.8–40°; sampling interval: 0.05°; counting time: 5 s. Fibers were tightly rolled up on aluminum sample holder (~0.5 × 2 cm^2) orthogonal to the incident beam.

Quasi-static tensile mechanical properties of the fibers were measured by an Instron ®4502 tensile testing machine, equipped with a load cell of 100 N. Single filaments with gage length of 30 mm were uniaxially drawn up to the break at 50 mm/min. According to ISO 527 standard, the elastic modulus was determined as a secant value between strain levels of 0.05% and 0.25%. For each samples 6 stress–strain curves were collected and averaged.

RESULTS AND DISCUSSION

As-spun Fibers

All composition were easy to spun in single monofilaments of 500 micron diameter, with a linear density of about 190 tex, as described in the previous paper.[35] Thermogravimetric analysis of fibers evidenced a shift of the degradation curve at higher temperature after introduction of LDH, as shown in Figure 1. Various comparative parameters such as the temperature of the selected mass loss, inflection point are summarized in Table II. As the most representative parameter appears the onset temperature of thermogram that proportionally increased from 356°C for the neat HDPE fiber up to 392°C for the fiber with 3% of LDH. Moreover, the inflection point is shifted from 423°C up to 442–460°C after incorporation of 0.5–3% of hydrotalcite, confirming the higher thermal stability of LDH-nanocomposite fibers.

SEM Analysis

SEM micrographs of the fracture surface of the fibers are reported in Figure 2. It could be seen that for LDH-1 [Figure 2(a,b)] and LDH-2 [Figure 2(c,d)] the dispersion of hydrotalcite was uniform. Mainly LDH particles clusters of about 0.25 μm are visible; however, single larger clusters in the range of 1.2–1.5 μm are also observed. At a higher magnification, the nanofiller particles seem to evidence a random distribution because of the irregular shape and the low aspect ratio. In contrast, the fracture surfaces of undrawn LDH-3 fibers reveal many clusters of

Table II. TGA Data of the Neat and Nanofilled HDPE Fibers

As spun fiber	Onset temperature [°C]	Temperature of 2% mass loss [°C]	Temperature of 5% mass loss [°C]	Max degradation rate [%/°C]	Inflection point [°C]
HDPE	356 ± 2.0	276 ± 2.0	333 ± 2.0	1.38	423
LDH-0.5	358 ± 1.0	268 ± 1.0	332 ± 3.0	1.16	456
LDH-1	365 ± 1.0	298 ± 3.0	344 ± 2.0	1.18	460
LDH-2	377 ± 5.0	294 ± 2.0	347 ± 1.0	1.22	460
LDH-3	392 ± 6.0	276 ± 3.0	377 ± 3.0	1.61	442

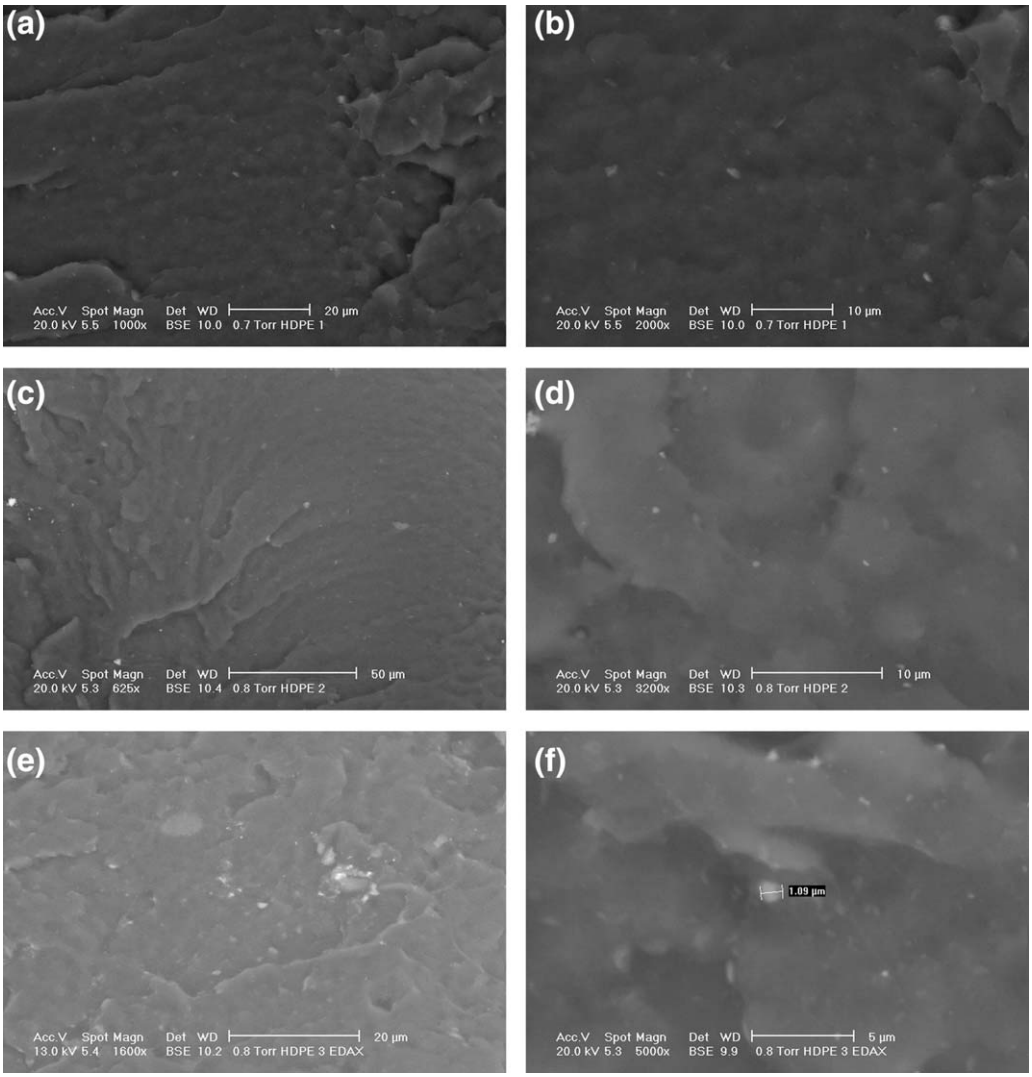

Figure 2. ESEM micrographs of LDH nanocomposite as-spun fibers (fracture surface). (a) LDH-1 (1000x); (b) LDH-1 (2000x); (c) LDH-2 (625x); (d) LDH-2 (3200x); (e) LDH-3 (1600x); (f) LDH-3 (5000x).

aggregates hydrotalcite particles with a mean size around 1.5–2 µm [Figure 2(e)]. It is known that for a low organoclay content a good dispersion of small size particles can be achieved, frequently at nanoscale, whereas higher loadings result in large size domains and less uniform distribution. Similar behavior was already observed by D'Amato et al. in the case of the HDPE-nanosilica composite fibres.[23]

Nonisothermal Crystallization Kinetics

In order to collect complementary information on the effect of crystallization temperature during drawing, a deeper investigation on the crystallization kinetics of HDPE nanocomposites analysis was performed. DSC results of the nonisothermal crystallization at different cooling rate between −0.3°C/min and −40°C/min are summarized in Table III. Higher crystallization

Table III. Crystallization Temperature (T_c) of the neat HDPE and HDPE Nanocomposites at Different Cooling Rate in DSC

	T_c (°C)							
Material	0.3°C/min	0.5°C/min	1°C/min	2°C/min	5°C/min	10°C/min	20°C/min	40°C/min
HDPE	124.3	123.8	122.6	120.7	117.6	111.3	107.5	99.8
LDH-0.5	124.3	123.6	122.2	119.7	115.8	112.2	102.5	91.1
LDH-1	124.2	123.6	122.7	121.3	118.6	112.4	110.0	101.3
LDH-2	123.9	123.3	122.3	121.3	118.7	113.0	110.0	101.2
LDH-3	123.9	123.5	122.6	121.1	118.4	115.1	110.0	103.7

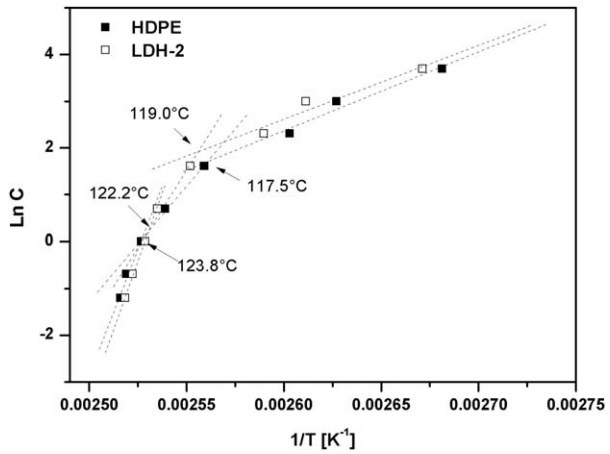

Figure 3. Plots of the cooling rate C (−K/min) versus crystallization temperature ($1/T_c$) for the neat HDPE and LDH-2 nanocomposite fibers. Dotted lines represent the best fitting of experimental datain arbitrary intervals; the intersections of the lines correspond to the transition temperatures between Regime I/Regime II and Regime II/ Regime III.

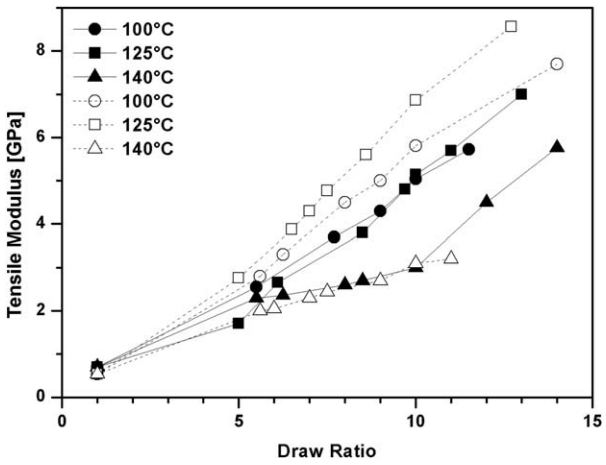

Figure 4. Tensile modulus of the neat HDPE (full symbols) and LDH-2 (empty symbols) fibers for various drawing temperature (circle-100°C, square-125°C, and triangle −140°C) as function of the draw ratio.

temperatures of the LDH nanocomposites seem to confirm a nucleating effect of hydrotalcite.[28,35]

The experimental data in three selected temperature intervals were fitted with straight lines whose slopes express the activation energy determined by using the Kissinger approach:

$$ln\,C = ln\,C_0 - \left(\frac{E_{act}}{R}\right) 1/Tc \qquad (3)$$

where C_0 is a pre-exponential factor, T_c is the peak temperature and R is the universal gas constant.[37] Figure 3 evidences the case of HDPE and LDH-2 for which the three straight lines could be related to the different mechanisms of the crystallization regimes I, II, and III of the Hoffman theory, and their intersection is related to the transition temperature between different regimes. For linear polyethylene, transition temperatures of 127°C and 119°C for regime I/II and regime II/III, respectively, were reported.[38] In our case, both transition temperatures and the activation energies of the regimes are summarized in Table IV. The transition temperatures for the neat HDPE ($T_{I/II} = 123.8$°C and $T_{II/III} = 117.5$°C) are slightly lower in comparison to literature data. In the case of HDPE/LDH nanocomposites $T_{I/II} \approx 122$°C, whereas the temperature transition between regime II and III was found at 119.0°C for LDH-1 and LDH-2. Moreover, the neat HDPE activation energies of 894, 410, and 140 kJ/mol for regime I, II, and III were calculated, respectively; whereas the calculated activation energies of regime I (about 1050 kJ/mol) and regime II (about 500 kJ/mol) of nanocomposites with 1–3% of LDH are higher than those of the neat HDPE. Such higher activation energy could be related to lower molecular mobility in the LDH nanocomposites, whereas a higher crystallization temperature could be attributed to the heterogeneous nucleation of hydrotalcite particles. Similar results were previously observed for the HDPE/$BaSO_4$ nanocomposites.[39] Thus, two different roles could be attributed to the LDH nanoparticles: first, they acted as nucleating agents and promoted the crystallization process of HDPE; second, they simultaneously acted as physical hindrances, thus retarding crystal growth of HDPE.[39]

Drawing Process

In our previous work, a preliminary drawing temperature 100°C was selected.[35] A deeper study on three drawing temperatures is presented in this paragraph; in particular both LDH-2 and HDPE fibers were drawn at 100°C, that is, the temperature of regime III crystallization, and at two higher temperatures, 125°C and 140°C, in the regime of crystallization type II and I.

Both elastic modulus and stress at break of fibers drawn at various temperatures are compared in Figures 4 and 5. The elastic modulus of the neat HDPE fibers with DR = 10 was found 3.0 GPa and 5.0 GPa after drawing at 140°C and at 100°C, respectively, whereas a value of 5.2 GPa was reached for drawing

Table IV. Transition Temperatures ($T_{I/II}$ and $T_{II/III}$) and Activation Energy of Crystallization (E_{act}) Found for Regimes I, II, and III for Neat HDPE and HDPE-LDH Composites

Composition	$T_{I/II}$ [°C]	$T_{II/III}$ [°C]	$E_{act\ I}$ [kJ/mol]	$E_{act\ II}$ [kJ/mol]	$E_{act\ III}$ [kJ/mol]
HDPE	123.8	117.5	894 ± 132	410 ± 25	140 ± 31
LDH-0.5	122.2	114.4	734 ± 77	320 ± 16	77 ± 5
LDH-1	122.7	119.0	1046 ± 30	496 ± 20	137 ± 25
LDH-2	122.2	119.0	974 ± 56	551 ± 30	131 ± 35
LDH-3	122.7	117.5	1175 ± 156	486 ± 42	149 ± 8

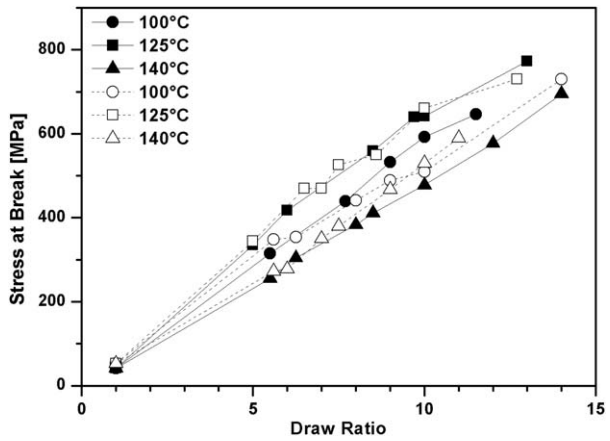

Figure 5. Stress at break of the neat HDPE (empty symbols) and LDH-2 (full symbols) fibers for various drawing temperature (square-100°C, circle-125°C, and triangle-140°C) as function of the draw ratio.

temperature of 125°C (Figure 4). In the case of LDH-2 fiber the same tendency was observed, with elastic modulus of 3.1 GPa after drawing ten times at 140°C, 5.8 GPa at 100°C and 6.9 GPa at 125°C.

Figure 5 shows similar trends for stress at break. For DR = 10, the neat HDPE fibers show the highest stress at break (640 MPa) for drawing temperature of 125°C; slightly lower values were found at 100°C (590 MPa) and 140°C (480 MPa). The trends observed for the LDH nanofilled fibers are quite analogous, (660, 470, 530 MPa, respectively).

The dependence of fiber mechanical properties on drawing temperature could be interpreted in term of crystallization-induced-orientation, and also taking into consideration the different crystallization forms and regimes, as briefly summarized by the description of Hoffman and coworkers.[38] In regime I, secondary nucleation rate is slow allowing for completion of the nucleated layer before the next event of the secondary nucleation; in the regime II, their rates are comparable to allow multiple nucleation; finally, during III regime surface spreading is lower than the nucleation rate. Hence, fibers drawn at the lower temperature (100°C) could developed further crystallization according to crystallization regime III, where the nucleation rate is slow, and thus, accounting for a lower crystallinity content. Moreover, in regime III zone a similar activation energy $E_{act\ III}$ of about 135 kJ/mol was found for both HDPE and LDH-2. The highest mechanical properties (Figures 4 and 5) were obtained for HDPE and LDH-2 fibers drawn at 125°C, where HDPE crystallized according to regime II and I, so that both nucleation and growth rates are comparable. At 140°C, crystallization proceeds owing mainly to the intense nucleation because the nucleation rate is higher than surface spreading, and hence, lower mechanical properties were achieved. These results, even those of LDH-2, are in agreement with data of HDPE fibers reported by Ward, where the highest elastic modulus and the draw ratio were achieved for drawing temperature close to 120°C. [7]

Characterization of Fibers Drawn at 125°C

Following our previous findings, 125°C was selected as drawing temperature for both HDPE and all other LDH nanocomposites, and an extensive study is reported in the next paragraphs, where XRD analysis and thermal and mechanical characterization are described.

XRD Analysis

The XRD analyses of the HDPE/LDH as-spun and selected drawn fibers are shown in Figure 6(a–c), in order to evaluate the extent of intercalation and exfoliation of the nanofiller. The

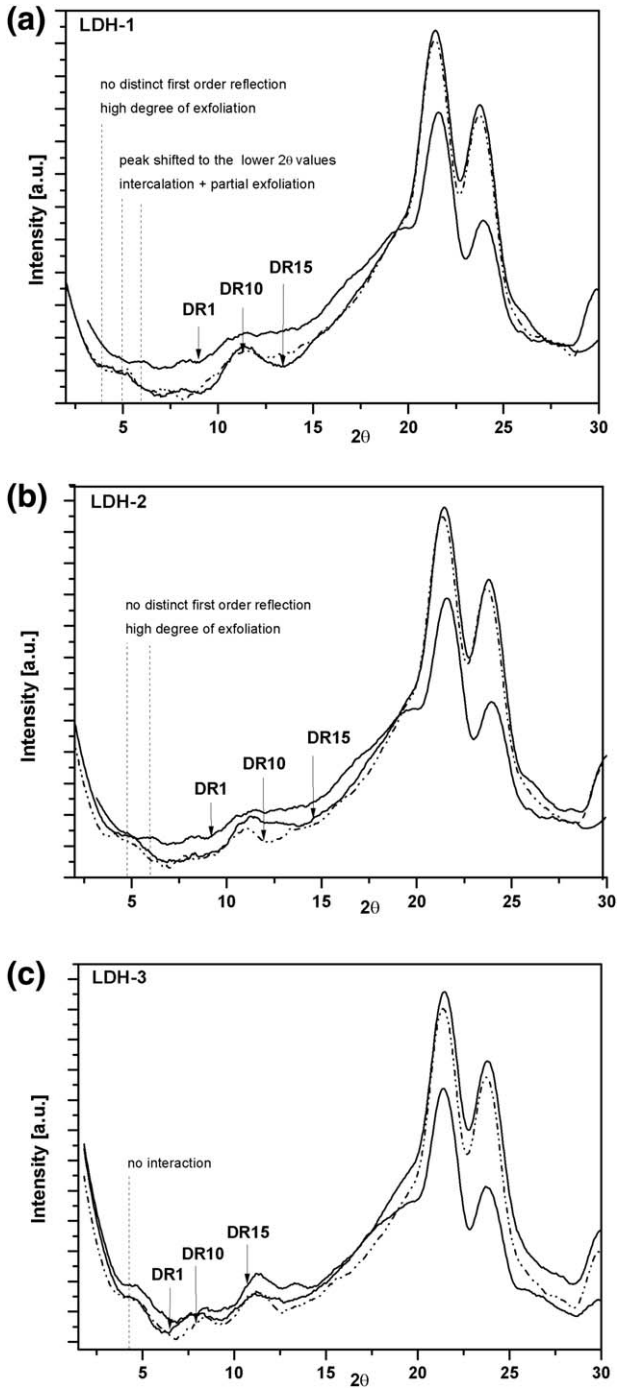

Figure 6. XRD patterns of the HDPE-LDH nanocomposite fibers for selected draw ratio (DR) at 125°C and different nanofiller content (a) LDH-1, (b) LDH-2, and (c) LDH-3.

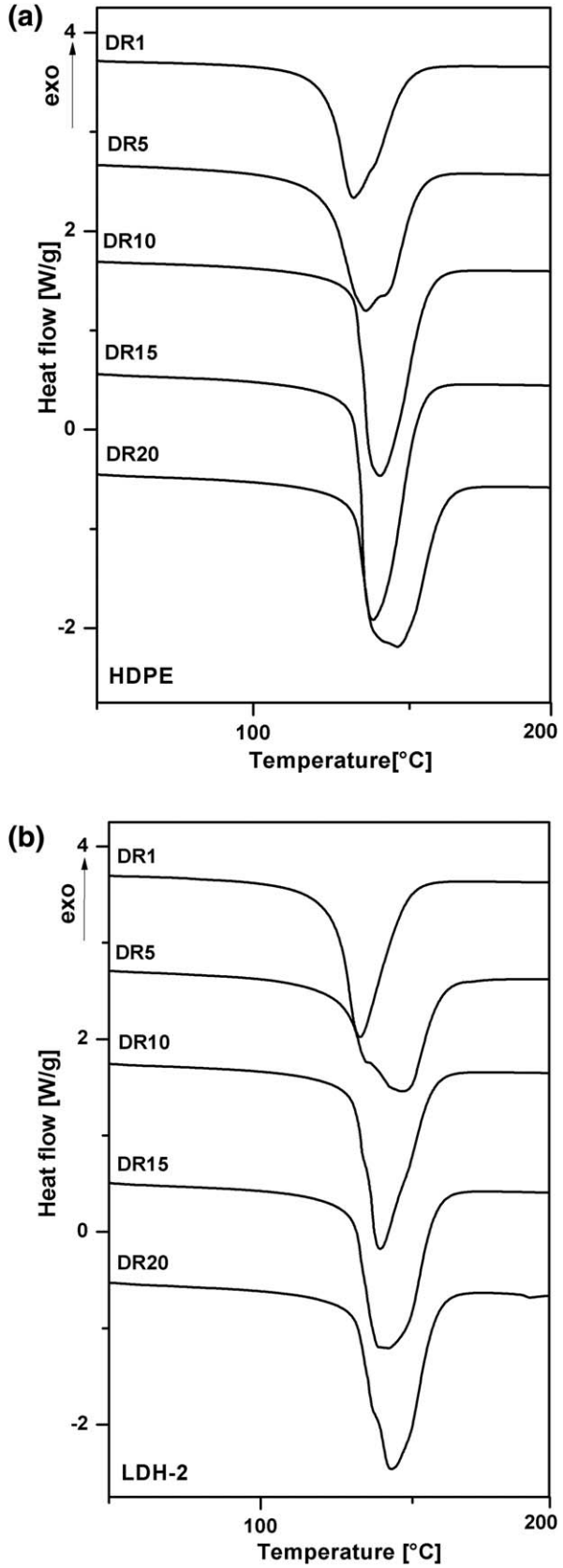

Figure 7. The first heating DSC thermograms of a) neat HDPE and b) LDH-2 nanocomposite fiber drawn at 125°C at selected draw ratio (DR).

XRD pattern were interpreted with respect to the position of the basal peak (003) of the hydrotalcite phase ($Mg_6Al_2(CO_3)(OH)_{16}{\cdot}4H_2O$, PDF card n. 41–1428), which depends on the distance between two adjacent metal hydroxide sheet in the LDH crystal lattice. The higher order peak of the same *hkl* series (006, 009) was also reported and both peaks indicate the presence of repeating crystal planes and symmetry in a specific crystallographic direction.[30] On the XRD spectra of LDH-1 nanocomposites, three characteristic Bragg reflections at about 6° (003), 8.1° (006), and 11.5° (009) of LDH presence can be observed [Figure 6(a)]. The first and the third can be univocally attributed to (003) and (006) reflexes of the reported reference phase, set at 5.48° and 11.27°, respectively. The second peak can be tentatively assigned to a minor Dypingite phase (ICPDS Powder Diffraction File card n. 23–1218), present in the starting mineral raw material. After the drawing process (DR = 10) the XRD patterns show change in the position of the basal reflection of the HDPE/LDH nanocomposites. For LDH-1 the peaks were shifted, respectively, from 6° up to 5.2° and 8.1° till 7.2° [Figure 6(a)]. As reported by other researchers, these results might suggest possible intercalation along with partial exfoliation.[30,40,41] In the case of LDH-2 the first basal reflections become very broad and the maximum of the bands, from 8.2° and 11.5°, shifts to lower 2θ, 7.8°, and 11.0° respectively, as compared with as-spun fiber [Figure 6(b)]. Moreover, in order to check the change in LDH intercalation/exfoliation process during drawing, XRD analyses for DR = 15 samples were also performed. In this case the first basal peak cannot be observed for both compositions LDH-1 and LDH-2, whereas the position of the other two peaks remains unchanged in comparison to DR10. This suggests that with further drawing the exfoliation process is more effective. In contrast, the results of LDH-3 were reported in Figure 6(c), and no change in the position of the three peaks was observed, even at high draw ratio. These findings suggested that nanoparticles in LDH-3 were not well dispersed and the formation of aggregates prevented the intercalation process.[40] Moreover, it is worth noting the increase of intensity of the peaks related to the polyethylene (21.4° and 23.7°) after drawing for all LDH composition. High enhancement of crystallinity content was obtained up to DR = 10, whereas after higher drawing (DR = 15) only minor variations were observed, in agreement with DSC analysis (see next paragraph). The overall XRD results confirmed that LDH layers were partially/fully separated with the formation of an intercalated/exfoliated.[42] It can be concluded that XRD analysis of HDPE nanocomposites fibers shows significant change in the position of the basal peak after drawing process. Moreover the disappearance of the (003) peak for LDH-1 and LDH-2 at DR = 15, suggested that LDH particles undergo more and more fragmentation during drawing process and lose their order structures to a great extent.[40]

Differential Scanning Calorimetry

DSC thermograms of the first heating scan for neat HDPE and LDH-2 nanocomposite fibers with different draw ratios are compared in Figure 7, while all results of the heating–cooling–heating cycle are summarized in Table V. Melting temperature of the as-spun HDPE and LDH nanocomposite fibers was found at 133°C, (Table V), whereas a higher crystallinity

Table V. Results of the DSC Analysis (1st heating–cooling–2nd heating): Crystallinity Content (χ) Melting Temperature (T_m), and Crystallization Temperatures (T_c) for Neat HDPE and HDPE Nanocomposite Fibers at Selected Draw Ratio (DR)

		1st Heating		Cooling		2nd Heating	
Material	DR	χ_1 [%]	T_{m1} [°C]	χ_c [%]	T_c [°C]	χ_2 [%]	T_{m2} [°C]
HDPE	1	50	133	65	111	65	143
	5	65	136	70	113	70	141
	10	70	140	68	114	68	138
	15	75	138	71	114	71	136
	20	74	146	71	111	71	140
LDH-0.5	1	52	133	70	112	70	142
	5	69	142	70	112	70	144
	10	70	142	70	113	70	141
	15	76	138	72	116	72	136
	20	75	140	71	109	71	137
LDH-1	1	53	133	68	112	68	142
	5	66	142	69	113	69	141
	10	69	141	66	114	65	140
	15	78	139	72	114	72	139
	20	77	140	74	112	74	140
LDH-2	1	54	132	66	113	66	141
	5	60	146	66	114	66	140
	10	66	144	66	114	66	140
	15	74	142	71	112	71	139
	20	74	143	71	114	71	139
LDH-3	1	53	133	69	115	69	137
	5	62	144	63	114	63	139
	10	68	143	65	116	65	139
	15	73	137	73	116	73	138
	20	74	140	73	116	73	138

content was detected for LDH fiber (52–54% vs 50% of neat HDPE), in conformity to literature data of polyolefin/clay nanocomposites.[13,43,44] The increase in fiber orientation upon solid-state drawing determined not only an increase in the melting temperature up to 140–146°C but also in the degree of crystallinity from about 50% up to 74–78%. The highest crystallinity content was found for LDH-1 (78% at DR15). The multiple melting peaks observed for fibers with DR = 5 (Figure 7), are related to the difference of crystal forms or the degree of their perfection obtained during drawing. The substantial increase of crystallinity of LDH composite fibers in comparison to neat HDPE was obtained for draw ratio between 5 and 10, reaching an almost plateau value for drawing 15–20. The degree of crystallinity of oriented samples follows a trend similar to that of the melting temperature, that is, both quantities increase with orientation and level off at higher degrees of molecular chain alignment.[45] In particular the orientation-induced crystallization, and typical folded-chain lamellar structure of flexible polymers convert into the extended–chain structure.[46] In the cooling step, the crystallization temperature of the as-spun LDH composite was found 1–4°C higher than that of the neat HDPE, confirming the role of hydrotalcite as nucleating agent, in conformity to other literature data[28,47] It can be concluded that during drawing at 125°C, the higher the draw ratio, the higher polymer chains orientation, and the higher crystallinity, particularly effective in the case of LDH-1 fiber.

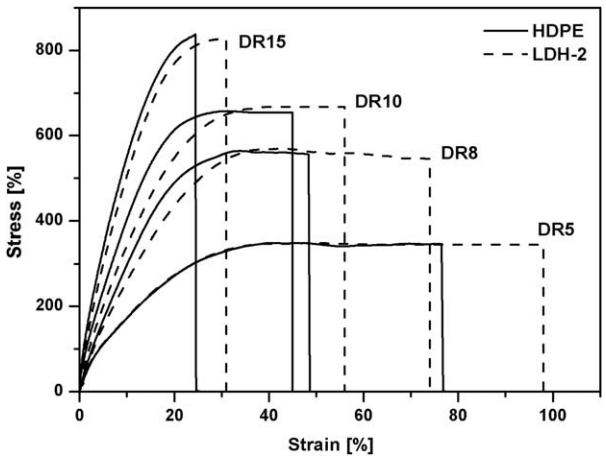

Figure 8. Representative stress–strain curves for neat HDPE and LDH-2 fiber drawn at 125°C with different draw ratio (DR).

Table VI. Mechanical Properties of Neat HDPE and Nanofilled HDPE Fibers at Selected Draw Ratio (DR)

Material	DR	Linear density[a] [tex]	Elastic modulus [GPa]	Stress at break [MPa]	Strain at break [%]	Tenacity[a] [cN/tex]	True strength[b] [MPa]	Mechanical draw ratio λ_{MEC}	Total draw ratio λ_{TOT}	Draw stiffening factor[c]
HDPE	1	187.2	0.55 ± 0.02	42 ± 1	1206 ± 20	4.4	549	13.1	142.2	1.0
	5	37.7	1.71 ± 0.23	335 ± 15	70 ± 10	36.8	570	1.70	91.4	3.1
	10	16.9	5.15 ± 0.25	642 ± 18	47 ± 4	67.5	963	1.47	177.8	9.4
	15	12.7	8.02 ± 0.55	842 ± 45	20 ± 4	87.2	1010	1.20	193.2	14.5
	20	9.1	9.80 ± 0.25	983 ± 40	16 ± 3	102.6	1179	1.16	261.0	17.8
LDH-0.5	1	185.4	0.53 ± 0.01	56 ± 4	1860 ± 60	5.9	1098	19.6	213.4	1.0
	5	38.0	1.94 ± 0.15	274 ± 17	105 ± 5	29.0	548	2.05	110.3	3.7
	10	16.9	5.45 ± 0.30	586 ± 25	43 ± 4	61.6	820	1.43	173.0	10.3
	15	12.8	8.86 ± 0.51	742 ± 15	27 ± 5	75.0	964	1.27	204.5	16.7
	20	9.2	10.0 ± 0.6	865 ± 13	17 ± 3	81.2	1040	1.17	263.2	18.8
LDH-1	1	188.4	0.60 ± 0.04	52 ± 6	1360 ± 60	5.4	759	14.6	158.9	1.0
	5	37.8	2.85 ± 0.13	340 ± 12	66 ± 12	36.7	578	1.66	89.3	4.8
	10	16.8	6.51 ± 0.45	680 ± 50	26 ± 7	71.0	884	1.26	152.5	10.8
	15	12.8	9.02 ± 0.31	786 ± 35	17 ± 6	79.4	943	1.17	188.4	15.0
	20	9.2	10.3 ± 0.5	865 ± 27	15 ± 2	80.0	951	1.15	258.7	16.3
LDH-2	1	191.5	0.62 ± 0.02	53 ± 1	1770 ± 42	5.4	991	18.7	203.6	1.0
	5	37.4	2.76 ± 0.15	344 ± 27	98 ± 17	38.0	688	1.98	106.5	4.5
	10	16.8	6.86 ± 0.51	661 ± 18	56 ± 14	70.2	1057	1.56	188.7	11.1
	15	12.7	9.27 ± 0.45	833 ± 52	27 ± 7	86.5	1083	1.27	204.5	15.0
	20	9.1	10.0 ± 0.5	964 ± 25	14 ± 3	95.6	1060	1.14	256.5	16.1
LDH-3	1	192.7	0.66 ± 0.02	43 ± 1	1470 ± 70	4.4	675	15.7	171.0	1.0
	5	37.5	2.31 ± 0.13	246 ± 20	98 ± 15	37.2	492	1.98	106.5	3.5
	10	16.8	6.04 ± 0.38	600 ± 14	52 ± 9	62.6	900	1.52	184.0	9.1
	15	12.7	8.51 ± 0.55	753 ± 18	21 ± 5	79.0	904	1.21	200.8	12.8
	20	9.1	10.3 ± 0.3	888 ± 15	20 ± 3	92.2	1065	1.20	270.0	15.6

[a] For definition of Linear density and Tenacity see ASTM.[48]
[b] Calculated according to eq. (6).
[c] Calculated as the ratio between the modulus of drawn fiber and the modulus of as-span fiber.

Mechanical Properties

Representative stress–strain curves of the neat HDPE and nanofilled polyethylene fibers at different draw ratio are reported in Figure 8, while the most relevant mechanical parameters are summarized in Table VI. It can be seen that fibers do not manifest a clear yield point at lower strains as usually observed for as-spun products. In fact, the drawing process produces a strong orientation of the macromolecules along the draw direction and the strain-induced crystallization of the amorphous regions, with a consequent increase in the fiber stiffness and the disappearance of yielding phenomena. These results are in conformity to previous researches, where a good dispersion enhanced the elastic modulus and the strength, and reduced the tensile ductility in comparison to neat matrix.[28,49]

Tensile modulus values at different draw ratios are summarized in Figure 9. It is worth noting that the stiffness of the nanofilled fibers notably increased with only a few weight percent of hydrotalcite. The highest improvement was obtained for LDH-1 and LDH-2 samples, whose tensile modulus at DR = 15 reached 9.0 GPa and 9.3 GPa, respectively, in comparison to 8.0 GPa of the neat HDPE.

The positive effect of the nanofiller on the tensile modulus can be explained by the percolation theory described by He and Jiang.[50] According to these authors, the matrix zone around each particle is affected by the stress concentration. If the distance between particles is small enough, these zones join together and form a percolation network which increases the modulus. For constant filler loadings, if the particles are fine and well dispersed, the total volume will be high, and the distance between the particles will be small. Therefore, the percolation network develops more easily and the modulus increases. The uniform nanofiller dispersion in case of compositions with 1 and 2 wt % of LDH was observed by SEM analysis [see Figure 2(a–d)].

The stiffening effect provided by LDH nanoparticles at various draw ratio is well documented by the relative tensile modulus E_R (Figure 10) according to the following equation:

$$E_R = \frac{E_{LDH}}{E_{HDPE}} \quad (4)$$

where E_{LDH} is the modulus of the nanocomposite fibers and E_{HDPE} is the modulus of HDPE fibers at the same draw ratio (data from Table VI). Relative modulus was found to increase with the nanofiller content reaching a relative maximum for LDH-1 and LDH-2, particularly significant at DR5 and DR10. Moreover, at the highest concentration of hydrotalcite (3 wt %), a lower stiffening effect (Figure 10) and modest increase of stress at break (Table VI) are especially visible for higher draw ratio (DR > 10). These effects can be explained in terms of filler dispersion, as reported by Costa et al. in the case of polyethylene/Mg-Al LDH nanocomposites, describing a critical concentration range of 2.5–5 wt % above which the LDH particles do not show strong interfacial adhesion with the matrix.[30] The existence of an optimal amount of the nanofiller was already observed by several authors.[15,17,19] In this article, the critical concentration of LDH in HDPE for fiber spinning was found at 2%. Above this concentration, hydrotalcite cannot be easily dispersed; clay will agglomerate in micrometric clusters acting as defects and stress concentration points that decrease drawability and polymer alignment.

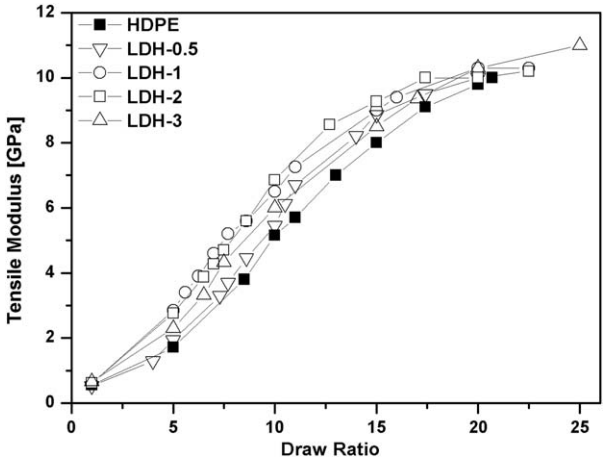

Figure 9. Tensile modulus of the neat and nanocomposite HDPE fibers with different amount of hydrotalcite as function draw ratio (DR) after drawing at 125°C.

It is well known that the mechanical properties of polymer fibers can be remarkably affected by the degree of crystallinity.[15,20] In Figure 11 tensile modulus at various DR and LDH content versus crystallinity content was plotted. It can be noted a proportional relationship between crystallinity content and tensile modulus. Drawn fiber of LDH-2 sample at high draw ratio reached the higher modulus values at relatively low crystallinity content, with respect to other fibers. This behavior suggests that the improvement in mechanical properties is related to various factors, such as the nanofiller content, orientation, and crystallinity that could play a synergistic role.

Stress at break values of the neat and nanofilled HDPE fibers were plotted versus draw ratio in Figure 12. Scientific literature showed various dependency of stress at break on nanofiller content, either increasing values after addition of 0.5–5 wt % of nanofiller, or unchanged, or even decreasing results, as in the case of nanofilled polypropylene fibers.[18,21,23,51] In this case, stress at break for LDH-1 and LDH-2 remained practically unchanged in comparison with that of neat HDPE fibers (Figure 12) up to DR15. Slightly lower values were found for the fibers with 0.5 wt % and 3 wt % of LDH.

Figure 13 shows the decreasing of strain at break values at the increase of draw ratio. All the compositions of as-spun HDPE-LDH fibers evidence higher strain at break than that of the neat HDPE fiber. With the higher draw ratio, strain at break decreases from about 1200% for as-spun HDPE and 1860% for LDH-0.5 up to 16% and 17%, respectively, for the fibers with DR = 20. As interpreted by Bilotti et al., the drawability of melt-crystallized flexible chain polymers achieved by drawing is limited by the presence of molecular entanglements.[52]

Some more information about spinnability and drawability could be obtained considering the mechanical draw ratio (λ_{MEC}), the true strength (σ^*_{MAX}), the processing draw ratio (λ_{PRO}), and the total draw ratio (λ_{TOT}) of selected fibers, as described in the followings and compared in Table VI.

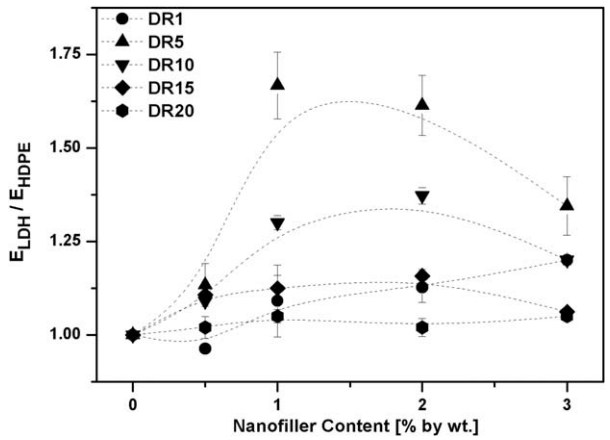

Figure 10. Relative tensile modulus of the HDPE-LDH nanocomposite fibers drawn at 125°C for different draw ratios.

The mechanical draw ratio (λ_{MEC}) is defined by eq. (5):

$$\lambda_{MEC}=(1+\varepsilon_b), \tag{5}$$

where ε_b is the strain at break. The true strength (σ_{MAX}) is calculated as the stress at break (σ_b) multiplied by the mechanical draw ratio [eq. (6)]:

$$\sigma_{MAX}=\sigma_b \quad \lambda_{MEC}=\sigma_b(1+\varepsilon_b). \tag{6}$$

Moreover, the processing draw ratio (λ_{PRO}) is defined as the ratio between the section of the die S_d and the section of the fiber S_f according to eq. (7):

$$\lambda_{PRO} = \frac{S_d}{S_f}. \tag{7}$$

And the total draw ratio (λ_{TOT}) has been calculated from eq. (8):

$$\lambda_{TOT}=\lambda_{PRO} \quad \lambda_{MEC} \tag{8}$$

which depends on both processing and mechanical drawing.[53]

For the as-spun fibers, higher true strength values were obtained for all the composites with hydrotalcite. For example, the true strength of LDH as-spun fibers is between σ_{MAX} = 675–1098 MPa and their total draw ratio from λ_{TOT} = 159–213, whereas

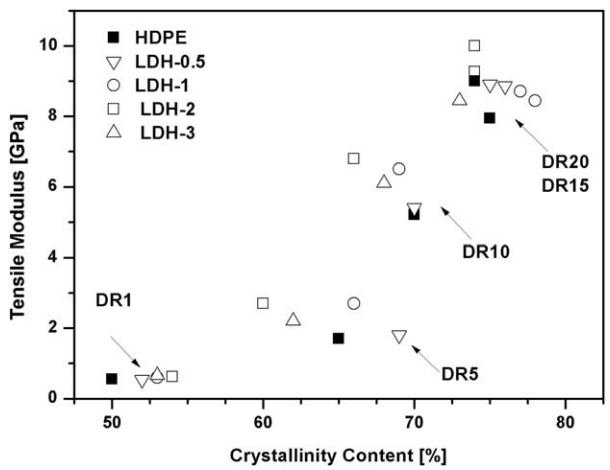

Figure 11. Tensile modulus of the neat and nanocomposite HDPE fibers drawn at 125°C as a function of the degree of polymer crystallinity.

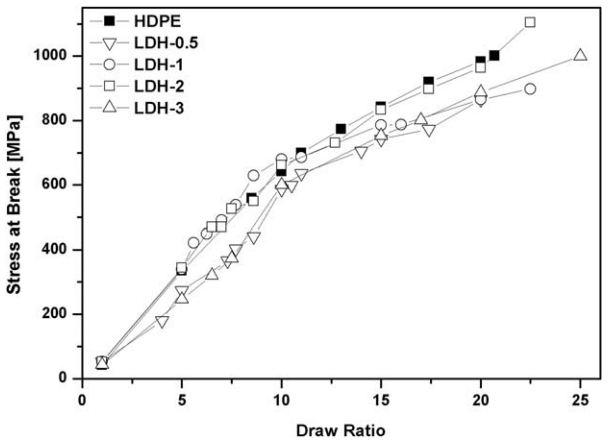

Figure 12. Stress at break of the neat and nanocomposite HDPE fibers with different amount of hydrotalcite as function draw ratio (DR) after drawing at 125°C.

the correspondent values of the neat HDPE as-spun fibers are 549 MPa and 142, respectively. In the case of drawn fibers, true strength and mechanical draw ratio are very similar for both neat and nanofilled HDPE fibers. Also, the total draw ratio indicates that LDH fiber could be spun and drawn at the same levels of HDPE fiber, confirming the good processability of hydrotalcite composites.

Moreover, a quantitative evaluation of the fiber properties and drawability of each composition could be remarked considering the draw-stiffening factor, calculated as the ratio between modulus of drawn fiber and modulus of as spun fiber, also reported in Table VI. These values are directly dependent on the draw ratio, and it is well evident the higher draw-stiffening factor of the LDH fiber containing 0.5–2% of hydrotalcite, with respect to the neat HDPE fiber up to DR15. Once again similar or lower values for LDH-3.

A complementary evaluation of the maximum attainable property P_∞ (either modulus or stress at break) could be calculated

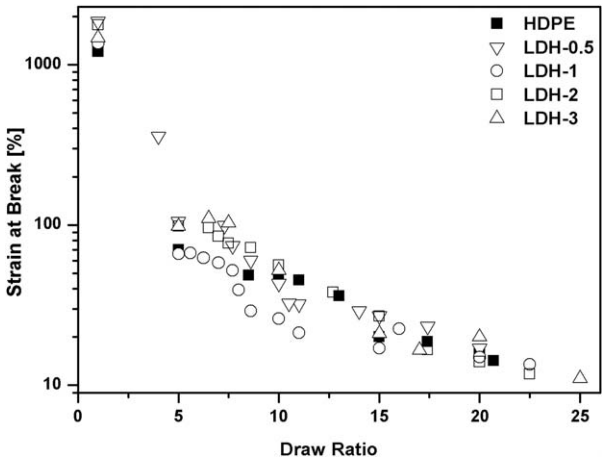

Figure 13. Strain at break of the neat and nanocomposites HDPE fibers with different amount of hydrotalcite as function of draw ratio (DR) after drawing at 125°C.

Table VII. Maximum Attainable Values of Elastic Modulus (E_∞) and Stress at Break (σ_∞) of Neat HDPE and LDH Nanocomposite Fibers, as Predicted from eq. (9).

Drawn fiber	E_∞ [GPa]	σ_∞ [MPa]
HDPE	11.8 ± 0.9	1180 ± 50
LDH-0.5	11.1 ± 0.8	1117 ± 26
LDH-1	11.8 ± 0.4	1029 ± 18
LDH-2	12.9 ± 0.2	1218 ± 56
LDH-3	13.2 ± 0.4	1205 ± 31

by the linear fitting of all experimental data P versus 1/DR according to the equation:

$$P = P_\infty - k_p 1/DR \quad (9)$$

where k_p is a proportionality constant taken into account the sensitivity of the property to the drawing.[54] Following this approach, predicted attainable strength of the compositions with 2 and 3 wt % of the filler (1218 ± 56MPa for LDH-2, and 1205 ± 31MPa for LDH-3) was slightly higher than 1180 ± 50 MPa of neat HDPE fiber, as presented in Table VII. Similar tendency was also observed in the case of the maximum attainable tensile modulus, that is, 12.9 GPa for LDH-2 and 13.2 GPa for LDH-3, with respect to 11.8 GPa of neat HDPE.

CONCLUSIONS

High density polyethylene (HDPE) and its composites with 0.5–3 wt % of organically modified hydrotalcite (LDH) were compounded and spun by combining melt-extrusion and hot-drawing at temperature between 100°C and 140°C. The most suitable drawing temperature was found to be 125°C for both the neat HDPE and nanocomposites. Fibers could be easily drawn at high draw ratios (up to 20) reaching linear density up of 9 tex and tensile modulus of about 10 GPa. In general, spinnability and drawability of the nanofilled polyethylene were found analogous to those of the neat HDPE.

The incorporation of LDH increased the thermal stability of composite fibers in comparison with HDPE. Moreover, crystallization kinetics indicates a nucleation effect of LDH on the HDPE matrix and evidences slightly enhanced temperature of the transition between Regimes II/III at 119°C for the composites containing 1–2% by wt % of LDH. Morphology and XRD analysis revealed a high degree of exfoliation of LDH in fibers containing 1–2% by weight of nanoclay, which was particularly evident after drawing. Consequently, tensile modulus of nanofilled fibers rose with the LDH content and drawing ratio. Tensile stress at break and strain at break of composite fibers approximately corresponded to those of the neat HDPE. Using the experimental data, a maximum value of elastic modulus of about 12.9–13.2 GPa was obtained through stiffness extrapolation of the nanofilled fibers containing 2–3% of LDH (with respect to 11.8 GPa found for the neat HDPE).

Practically, the addition of nanoparticles has been found advantageous in terms of improvement of the thermal stability, and favorable for developing at least the same mechanical performances of polyethylene matrix. These beneficial effects can be attributed to a good dispersion of hydrotalcite particles, which promote molecular orientation and crystallization in the HDPE matrix and also act as thermal barriers.

ACKNOWLEDGMENTS

The authors thank Dr. Giuseppe Ferrara (LyondellBasell Industries-Basell Poliolefine Italia S.r.l. "Giulio Natta" R&D) for helpful suggestions and Clariant Masterbatches S.p.A. (Italy) for donating the HDPE perkalite masterbatch. The authors are also very indebted to professor Jan Kolarik (Institute of Macromolecular Chemistry, Prague) for his valuable comments.

REFERENCES

1. Treloar, L. R. G., *Polymer* **1960**, *1*, 95.
2. White, J. L.; Dharod, K. C.; Clark, E. S. *J. Appl. Polym. Sci.*, **1974**, *18*, 2539.
3. Andrews, J. M.; Ward, I. M. *J. Mater. Sci.*, **1970**, *5*, 411.
4. Capaccio, G.; Ward, I. M. *Polymer* **1974**, *15*, 233.
5. Capaccio, G.; Crompton, T. A.; Ward, I. M. *Polymer* **1976**, *17*, 644.
6. Vlasblom, M. P.; Van Dingenen, J. L. J. In Handbook of Tensile Properties of Textile and Technical Fibres; Bunsell, A. R., Schwartz, P., Eds.; Woodhead Publishing in Textiles, TJ International Ltd.: Padstow, Cornwall (UK), **2009**; Chapter *13*, pp 437–485.
7. Ward, I. M.; Lemstra, P. J. In Handbook of Textile Fibre Structure: Fundamentals and Manufactured Polymer Fibres; Eichhorn, S. J.; Hearle, J. W. S.; Jaffe, M.; Kikutani, T., Eds.; Woodhead Publishing in Textiles, TJ International Ltd.: Padstow, Cornwall (UK), **2009**; Vol. *1*, Chapter *12*, pp 352–393.
8. Capaccio, G.; Ward, I. M. *Polymer* **1975**, *16*, 239.
9. Perkins, W. M.; Capiati, N. J.; Porter, R. S. *Polym. Eng. Sci.*, **1976**, *16*, 200.
10. Smith, P.; Lemstra, P. *J. Mater. Sci.*, **1980**, *15*, 505.
11. Ward, I. M. *Plast. Rubber. Compos.*, **2004**, *33*, 189.
12. Gupta, R. K.; Kennel. E. B.; Kwang-Jea, K. In Polymer Nanocomposites Handbook; Gupta, R. K., Kennel. E. B., Kwang-Jea, K., Eds.; Taylor and Francis Group: Boca Raton, **2010**; Chapter *1*, pp 22–44.
13. Xiuqin, Z.; Mingshu, Y.; Ying, Z.; Shimin, Z.; Xia, D.; Xuexin, L.; Dujin, W.; Duanfu, X. *J. Appl. Polym. Sci.*, **2004**, *92*, 552–558.
14. Joshi, M.; Viswanathan, V. *J. Appl.Polym. Sci.*, **2006**, *102*, 2164.
15. Lee, S. H.; Youn, J. R. *J. Appl. Polym. Sci.*, **2008**, *109*, 1221.
16. Rottstegge, J.; Zhang, X.; Zhou, Y.; Xu, D.; Han, C. C.; Wang, D. *J. Appl. Polym. Sci.*, **2007**, *103*, 218.
17. Soitong, T.; Pumchusak, J. *J. Mater. Sci.*, **2011**, *46*, 1697.
18. Lorenzi, D.; Sartori, G.; Ferrara, G.; Fambri, L. *Macromol. Symp.*, **2011**, *301*, 73.
19. Rattanawijan, W.; Amornsakchai, T. *J. Appl. Polym. Sci.*, **2012**, *124*, 501.

20. Sulong, A. B.; Park, J.; Azhari, C. H.; Jusoff, K. *Compos. Part B-Eng.*, **2011**, *42*, 11.
21. La Mantia, F. P.; Dintcheva, T. N.; Scaffaro, R.; Marino, R. *Macromol. Mater. Eng.*, **2008**, *293*, 83.
22. La Mantia, F. P.; Marino, R.; Dintcheva, T. N. *Macromol. Mater. Eng.*, **2009**, *294*, 575.
23. D'Amato, M.; Dorigato, A.; Fambri, L.; Pegoretti, A. *Exp. Polym. Lett.*, **2012**, *6*, 954.
24. Wang, K. H.; Xu, M.; Choi, Y. S.; Chung, I. *J. Polym. Bull.*, **2001**, *46*, 499.
25. Zhang, Y.; Yu, J.; Zhou, C.; Chen, L.; Hu, Z. *Polym. Composite.*, **2010**, *31*, 684.
26. Wang, D.-Y.; Das, A.; Leuteritz, A.; Boldt, R.; Häußler, L.; Wagenknecht U.; Heinrich, G. *Polym. Degrad. Stab.*, **2011**, *96*, 285.
27. Purohit, P. J.; Wang, D.-Y.; Emmerling, F.; Thünemann, A. F.; Heinrich, G.; Schönhals, A. *Polymer*, **2012**, *53*, 2245.
28. Marega, C.; Causin, V.; Marigo, A.; Ferrara, G.; Tonnaer, H. *J. Nanosci. Nanotechnol.*, **2009**, *9*, 2704.
29. Costa, F. R.; Abdel-Goad, M.; Wagenknecht, U.; Heinrich, G. *Polymer*, **2005**, *46*, 4447.
30. Costa, F. R.; Satapathy, B. K.; Wagenknecht, U.; Weidisch, R.; Heinrich, G. *Eur. Polym. J.*, **2006**, *42*, 2140.
31. Longzhen, Q.; Wei, C.; Baojun, Q. *Polymer*, **2006**, *47*, 922.
32. Wei, C.; Baojun, Q. *J. Mater. Chem.* **2004**, *14*, 1705.
33. Wang, Q.; Zhang, X.; Wang, C. J.; Zhu, J.; Guo, Z.; O'Hare, D. *J. Mater. Chem.* **2012**, *22*, 19113.
34. Guo, Z.; Hagström, B. *Polym. Eng. Sci.* **2013**, 53, 2035.
35. Dabrowska, I.; Fambri, L.; Pegoretti, A.; Ferrara, G. *Exp. Polym. Lett.*, **2013**, *7*, 936.
36. Van Krevelen, D. W. Properties of Polymers, 3rd ed.; Elsevier: Amsterdam, **1990**.
37. Kissinger, H. E. *J. Res. Natl. Bur. Stand.*, **1956**, *57*, 217.
38. Hoffman, J.; Miller, R. L. *Polymer*, **1997**, *33*, 3151.
39. Chen, X.; Wang, L.; Liu, Y.; Shi, J.; Shi, H. *Polym. Eng. Sci.*, **2009**, *12*, 2342.
40. Costa, F. R.; Leuteritz, A.; Meinl, J.; Wagenknecht, U.; Heinrich, G. *Macromol. Symp.*, **2011**, *301*, 46.
41. Ye, L.; Wu, Q. *J. Appl. Polym. Sci.*, **2012**, *123*, 316.
42. Lonkar, S. P.; Therias, S.; Leroux, F.; Gardette J.-L.; Singh, R. P. *Polym. Eng. Sci.*, **2012**, *52*, 2006.
43. Deshmane, C.; Yuana, Q.; Perkins, R. S.; Misra, R. D. K. *Mat. Sci. Eng. A-Struct.*, **2007**, *458*, 150.
44. Chantrasakul, S.; Amornsakchai, T. *Polym. Eng. Sci.*, **2007**, *47*, 943.
45. Clements, J.; Capaccio, G.; Ward, I. M. *J. Polym. Sci.: Polym. Phys.*, **1979**, *17*, 693.
46. Jaffe, M.; Menczel, J.D.; Bessey, W. E. In Thermal characterization of polymeric materials; Turi, E.A. Ed.; 2nd edition, Academic Press, San Diego, **1981**; Vol. *2*, Chapter 7, pp 1767–1954.
47. Marega, C.; Causin, V.; Neppalli, R.; Saini, R.; Ferrara, G.; Marigo, A. *Exp. Polym. Lett.*, **2011**, *5*, 1050.
48. ASTM D123-13a: Standard terminology relating to textile 2013. Developed by Subcommittee: D13.92 DOI: 10.1520/D0123.
49. Hippi, U.; Mattila, J.; Korhonen, M.; Seppala, J. *Polymer* **2003**, *44*, 1193.
50. He, D.; Jiang, B. *J. Appl. Polym. Sci.*, **1993**, *49*, 617.
51. Dintcheva, N. T.; Marino, R.; La Mantia, F.P. *E-Polym.*, **2009**, 054.
52. Bilotti, E.; Deng, H.; Zhang, R.; Lu, D.; Bras, W.; Fischer, H. R.; Peijs, T. *Macromol. J.*, **2010**, *295*, 37.
53. Tomka J. G. In Comprehensive Polymer Science; Booth C., Price C., Eds.; Pergamon Press: Oxford, **1989**; Vol. *2*, Chapter 14, pp 487–510.
54. Fambri, L.; Bragagna, S.; Migliaresi, C. *Macromol. Symp.* **2006**, *234*, 20.